JCTC Journal of Chemical Theory and Computation

Article

pubs.acs.org/JCTC

Specific Reaction Path Hamiltonian for Proton Transfer in Water: Reparameterized Semiempirical Models

Xin Wu,[†] Walter Thiel,*[,†] Soroosh Pezeshki,[‡] and Hai Lin*[,‡]

[†]Max-Planck-Institut für Kohlenforschung, 45470 Mülheim an der Ruhr, Germany

[‡]Chemistry Department, University of Colorado, Denver, Denver, Colorado 80217, United States

Supporting Information

ABSTRACT: The semiempirical MNDO-based AM1 and PM3 methods and the orthogonalization-corrected OM1, OM2, and OM3 models were reparameterized to improve their description of bulk water and of proton transfer in water. Reference data included the gas-phase geometries and energies of the water molecule, small water clusters, the hydronium ion, and small hydronium ion−water clusters, as well as the gas-phase potential energy surface for proton transfer between the two water molecules in a Zundel ion, all calculated at the MP2/aug-cc-pVTZ level of theory. Combined QM/MM molecular dynamics simulations were carried out for bulk water and for a proton solvated in water using large cluster models. Both the authentic and reparameterized semiempirical models were employed in the simulations. The reparameterization led to significantly better results in all cases. The new set of OM3 parameters gave the best overall results for the structural and dynamic properties of water and the hydrated proton, with a small but finite barrier of 0.1−0.2 kcal/mol in the potential of mean force for proton transfer, in agreement with ab initio path-integral molecular dynamics simulations. The reparameterized OM3 model is expected to be useful for efficient modeling of proton transfer in aqueous solution.

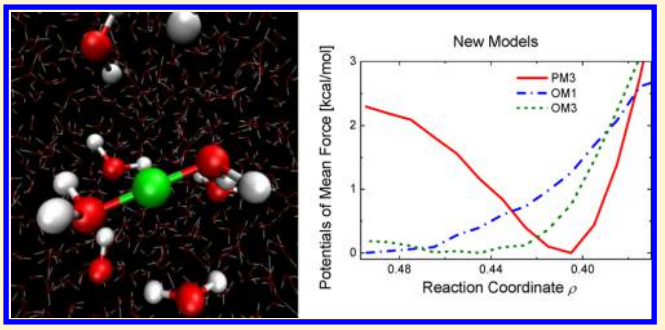

1. INTRODUCTION

Transfer of the hydrated proton in bulk water is very important in many chemical and biological processes.[1] The proposed Grotthuss shuttling mechanism,[2] which involves reorganization of the covalent and hydrogen bonds over time, presents a challenge in molecular dynamics (MD) simulations. The published studies can be largely divided into four categories, according to how the potential energies were determined. The first category of studies employed classical force fields that were specially designed to describe water dissociation, for example, the central force field by Stillinger and David[3,4] and its modification by Halley et al.,[5] the protonizable water model by Billeter and van Gunsteren,[6] the polarizable and dissociable water potential by Lussetti et al.,[7] the dissociative water potential by Mahadevan and Garofalini,[8] the ReaxFF reactive force field by van Duin and co-workers,[9] the reactive molecular dynamics (RMD) approach by Selvan et al.,[10] and the LEWIS reaction force field by Herzfeld and co-workers.[11] The second group of studies were based on the so-called multistate empirical valence bond (MS-EVB) model,[12] which is an extension of Warshel's EVB model.[13] Several parametrized two-state EVB and MS-EVB models for proton transfer in water were proposed by Voth and co-workers,[12,14−17] by Vuilleumier and Borgis,[18,19] by Tuckerman and co-workers,[20,21] by Kornyshev et al.,[22] and by Paesani and co-workers.[23] The third approach made use of ab initio molecular dynamics (AIMD), in particular, Car−Parrinello molecular dynamics (CPMD),[24] simulations using density functional theory (DFT) to compute the potential on the fly. The first such studies by Tuckerman et al.[25,26] in 1994 were followed by many similar publications.[1,16,17,27−34] The fourth type of simulations employed semiempirical methods, in particular, the self-consistent-charge density functional tight-binding (SCC-DFTB)[35] approach; this includes the work by Choi and Jordan,[36] by Maupin et al.,[37] and by Cui and co-workers.[38,39] All these studies have provided valuable insight into the solvation structure and the transport mechanism of the hydrated proton. It is commonly agreed that the proton transfer occurs via an Eigen−Zundel−Eigen mechanism, where the Eigen ion is the resting state and the Zundel ion is the transition state. However, some groups have also advanced different views (see, for example, refs 27 and 33, as well as the discussion in ref 17). Furthermore, based on the analysis of ab initio MD simulations, Berkerbach et al.[34] proposed a concerted mechanism, in which the rate-limiting step to proton diffusion is the loss of an acceptor hydrogen bond at the proton-receiving water molecule with concomitant formation of a hydrogen bond at the lone-pair site of the hydronium ion.

Semiempirical quantum-chemical methods are computationally much more efficient than ab initio or DFT methods, making them attractive choices for MD simulations. However,

Received: March 20, 2013
Published: May 3, 2013

the existing standard semiempirical models are generally not accurate enough in describing interactions between water molecules, or proton transfer barriers, or both. This calls for a revision of these models as a prerequisite for using them in simulations of water and aqueous solutions. One option is to add empirical dispersion corrections and/or hydrogen-bonding corrections, which has been attempted, for example, by McNamara and Hillier,[40] Hobza and co-workers,[41] Maupin et al.,[37] and Korth.[42,43] Hydrogen-bonding corrections have recently also been included by Cui and co-workers[39] into a new SCC-DFTB model that features third-order terms in the Taylor expansion of the charge fluctuations.[44]

In this paper, we report a specific reaction parametrization (SRP)[45] of two sets of established semiempirical methods that targets proton transfer in water. The first set includes the popular Austin Model 1 (AM1) by Dewar et al.[46] and the Parameterized Model 3 (PM3) by Stewart,[47,48] which are based on the Modified Neglect of Differential Overlap (MNDO) approximation by Dewar and Thiel.[49] The second set covers the family of orthogonalization-corrected model OMx (x = 1, 2, and 3) developed by Thiel and co-workers.[50−54] In all cases, the theoretical framework of the underlying semiempirical method was retained (i.e., no additional terms were introduced). Our goal was to develop specific semiempirical models that can reproduce ab initio calculated potential surfaces with reasonable accuracy, in order to enable efficient simulations of proton transfer in water. The reference data and the parametrization process are described in Section 2. Section 3 discusses the results, and conclusions are drawn in Section 4.

2. COMPUTATIONAL DETAILS

2.A. Parameterization. For the parametrization, we employed two groups of reference data calculated at the MP2 level of theory[55] with the aug-cc-pVTZ[56,57] basis set. The first group consisted of the fully optimized gas-phase geometries and the associated energies for water H_2O, water clusters $H_{2n}O_n$ (n = 2−5), the hydronium ion H_3O^+, and protonated water clusters $H_{2m+1}O_m^+$ (m = 2−4). The model systems are displayed in Figure 1; entries (a)−(g) are included in the training set and entries (h)−(j) are part of the validation set. For large clusters such as the water tetramer and pentamer, which have many close-lying local minima, we only selected the global minimum, with the initial geometries for optimization being taken from refs 58 and 59. We also computed the vibrational frequencies for these model systems as part of our assessment of the accuracy, but we did not attempt to reproduce these frequencies during the parametrization. The second group of reference data consisted of 99 data points on the two-dimensional potential energy surface for the transfer of one proton between two water molecules within the Zundel ion in the gas phase, computed by relaxed surface scans (Figure 2). In these surface scans, the distance between the oxygen atoms (R_{OO}) and the distance between the migrating proton and one oxygen atom were kept fixed in partial geometry optimizations. The 53 data points obtained for R_{OO} = 2.2, 2.4, 2.6, and 2.8 Å were included in the training set, whereas the other 46 data points for R_{OO} = 2.3, 2.5, 2.7, and 2.9 Å were employed for validation. Please note that the 99 data points are not uniformly distributed.

Semiempirical methods have traditionally been parametrized to reproduce experimental heats (enthalpies) of formation. The experimental heat of formation for water (−57.80 kcal/mol)[60] thus serves as the reference energy for water, i.e., entry (a) in

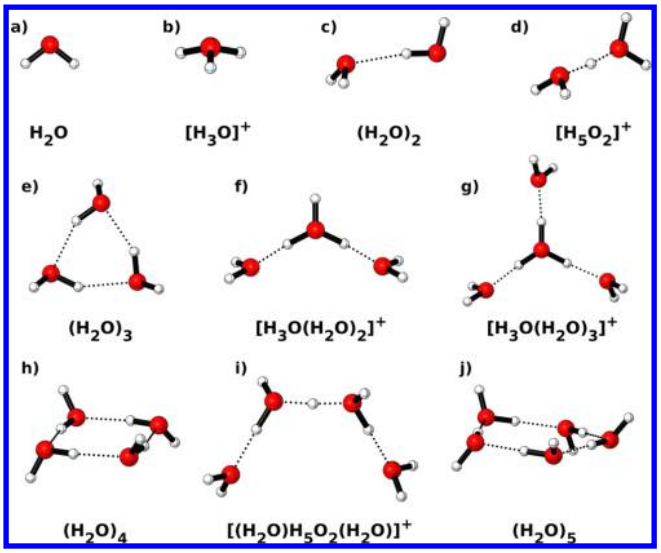

Figure 1. Neutral water clusters and protonated water clusters used for parametrization; entries (a)−(g) belong to the training set, and entries (h)−(j) are part of the validation set. Geometries were optimized at the MP2/aug-cc-pVTZ level.

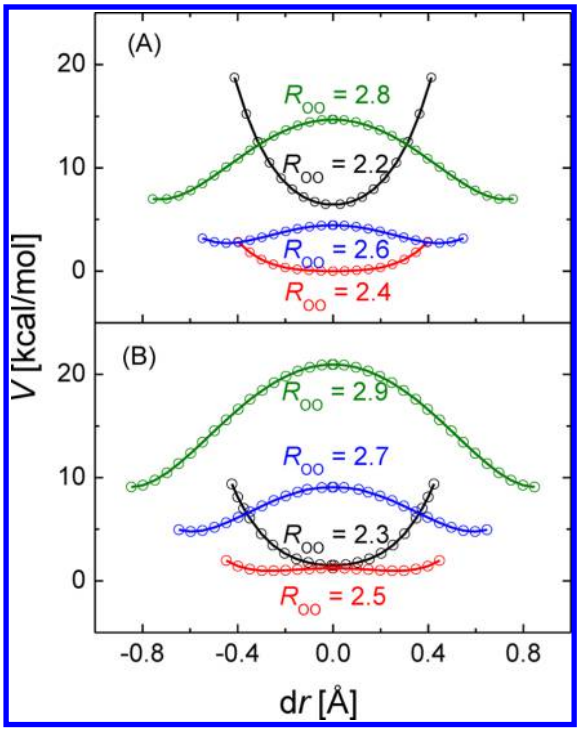

Figure 2. Reference MP2/aug-cc-pVTZ gas-phase energies (V) for proton transfer in the Zundel ion at fixed distances R_{OO} (in Ångstroms) obtained from relaxed surface scans ((A) training set and (B) validation set). Here, dr is the difference in the distances between the migrating proton and the two O atoms.

Figure 1. The target energies for all other systems are the corresponding ab initio binding energies. In the case of the water dimer (H_4O_2), the semiempirically computed energies (E^{SE}) should thus reproduce as closely as possible the binding energy calculated from their ab initio counterparts (E^{AI}), with the goal being

$$E^{SE}(H_4O_2) - 2E^{SE}(H_2O) = E^{AI}(H_4O_2) - 2E^{AI}(H_2O) \quad (1)$$

dx.doi.org/10.1021/ct400224n | J. Chem. Theory Comput. 2013, 9, 2672−2686

This equation can trivially be generalized to water *n*-mers. For the protonated water clusters, the semiempirical energy of the proton [i.e., experimental (or accurate) heat of formation for proton $\Delta H(H^+)$] is needed to compute the relative energies. In the case of the hydronium ion (H_3O^+), the target is

$$E^{SE}(H_3O^+) - E^{SE}(H_2O) - \Delta H(H^+) = E^{AI}(H_3O^+) - E^{AI}(H_2O) - E^{AI}(H^+) \quad (2)$$

where the electronic energy of an isolated proton $E^{AI}(H^+)$ is, by definition, zero. As is common in semiempirical work, we have used the value of 365.7 kcal/mol from ref 61 for $\Delta H(H^+)$. The target energies for the other protonated water clusters can be derived in the same way.

The ab initio reference calculations were carried out by using the *Gaussian09* package.[62] The semiempirical calculations and parametrizations were performed by using the MNDO package,[63] except for the PM6 calculations,[64] which were determined using *Gaussian09*. Reparameterizations were attempted for AM1, PM3, OM1, OM2, and OM3, and the resulting new models are denoted AM1*n*, PM3*n*, OM1*n*, OM2*n*, and OM3*n*, respectively. The following weights were employed in evaluating the error function for the parametrization: 10.0 $(kcal/mol)^{-1}$ for energy, 100.0 $Å^{-1}$ for distances, and 5.0 deg^{-1} for angles. We did not perform any extensive search for global minima in parameter space, because we wanted to keep the new parameters as close to the authentic parameters as possible.

2.B. Tests and Validation. The reparameterized semiempirical models were tested by doing calculations on a series of model systems. First, we examined the gas-phase binding energy profiles for two water molecules as a function of the distance between the two O atoms. The ab initio reference curve for the binding energy was computed at the MP2/aug-cc-pVTZ level by relaxed surface scans using *Gaussian09*,[62] in which the distance between the O atoms was changed by 0.1 Å from the previous geometry and then fixed during geometry optimization. The relaxed surface scan started from the fully optimized water dimer geometry and moved in both directions, toward longer and shorter O−O distances. The MP2 optimized geometries along this path were then adopted as input geometries for the semiempirical calculations using the MNDO program.[63]

Second, we carried out MD simulations for bulk water and for a hydrated proton in bulk water using large cluster models. Figure 3 depicts the model system for the hydrated proton. The entire system had a radius of R_{system} = 22 Å, containing 1482 water molecules and one hydronium ion initially placed at the center. The density was 1.00 g/mL. The system was divided into two regions: an inner core ($R_{inner} \leq 12$ Å) containing 240 water molecules plus the hydronium ion and an outer layer. The water molecules in the outer layer were subjected to harmonic potentials with force constants of 10 kcal mol^{-1} $Å^{-2}$ that restrained the atoms to their original positions and effectively prevented the water molecules from evaporating into the vacuum. The cluster model for neutral bulk water simulations was obtained by deprotonation of the hydronium ion.

Regarding the update of the hydronium O atom index, we have adopted the scheme proposed by Hofer et al.[65] As illustrated in Figure 4A, the donor (hydronium oxygen) is labeled O0. Any water oxygen atom ($O1_i$) within 2.9 Å from O0 will be enlisted as a potential acceptor; the number of potential acceptors varies over time during the MD simulations and can be larger than 3. For each potential acceptor $O1_i$ and each hydronium hydrogen H_j (j = 1, 2, and 3), a parallel vector component $\mathbf{R}^{//i}_{O0Hj}$ is computed by projecting the donor-

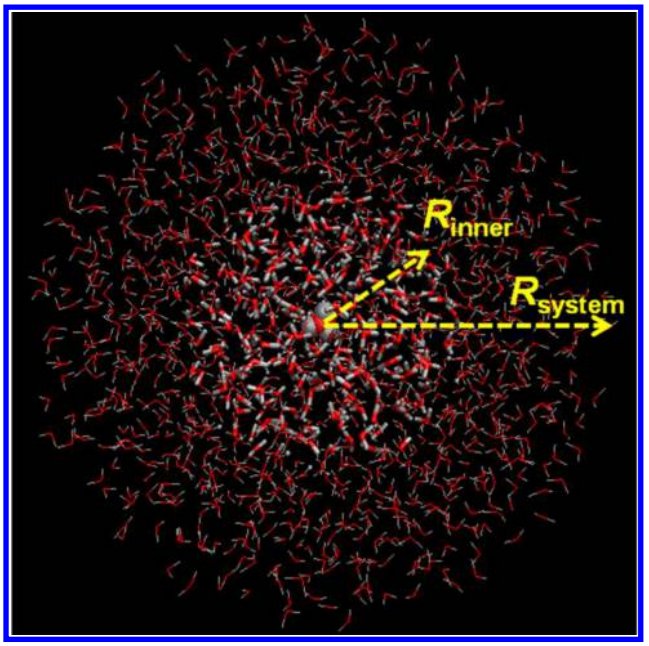

Figure 3. Cluster model for dynamics simulations of protonated water. The entire system has a radius of R_{system} = 22 Å, containing 1482 water molecules and one hydronium ion initially placed at the center. It is divided into an inner core ($R_{inner} \leq 12$ Å) containing 213 water molecules (licorice) plus the hydronium ion (van der Waals balls) and an outer layer with the other water molecules (lines). (See Section 2.B for further details.) The cluster model for the charge-neutral water simulations was generated by deprotonating the hydronium ion.

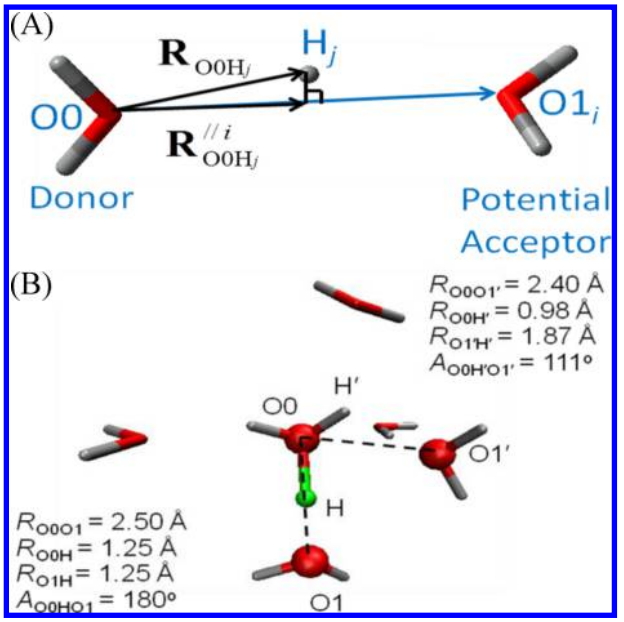

Figure 4. (A) Illustration of the criterion for donor−acceptor swaps during proton migration. (See Section 2.B for a detailed description.) (B) A snapshot of a donor−acceptor swap from an OM3*n* trajectory. H (in green) is the proton being transferred between O0 and O1, while H′ is the hydrogen between O0 and the nearest potential acceptor O1′. Note that the acceptor O1 is further away from O0 than O1′ is from O0.

dx.doi.org/10.1021/ct400224n | J. Chem. Theory Comput. 2013, 9, 2672−2686

Table 1. Parameters Re-optimized in This Work for the MNDO-Based Methods AM1 and PM3[a]

	AM1		PM3	
parameter	H	O	H	O
U_{ss} (eV)	−11.396 248 28	−97.830 051 00	−13.072 844 90	−86.946 179 86
U_{pp} (eV)		−78.262 408 38		−71.908 402 68
ζ_s (au)	1.188 187 56	3.107 792 05	0.954 530 51	3.757 723 92
ζ_p (au)		2.523 560 51		2.404 027 00
β_s (eV)	−6.173 824 58	−29.272 769 70	−5.618 505 74	−45.206 662 11
β_p (eV)		−29.272 857 32		−24.733 236 26
α (Å^{-1})	2.882 439 11	4.455 399 50	3.374 889 68	3.219 112 53
G_{ss} (eV)	12.847 854 58	15.419 913 68	14.809 518 87	15.777 238 66
G_{pp} (eV)		14.520 099 32		13.598 867 86
G_{sp} (eV)		14.479 690 53		10.621 326 89
G_{p^2} (eV)		12.979 865 09		12.449 747 02
H_{sp} (eV)		3.939 834 42		0.578 426 14
K_1	0.122 538 40	0.280 798 02	1.047 892 68	−1.074 471 74
L_1	4.999 771 05	5.000 022 09	5.142 074 74	5.949 950 70
M_1	1.199 850 35	0.847 737 05	1.556 607 86	1.600 454 10
K_2	0.004 892 58	0.081 222 13	−1.022 154 81	1.109 274 09
L_2	4.999 919 96	7.000 037 71	5.984 287 97	5.926 025 97
M_2	1.800 222 36	1.444 973 83	1.563 919 61	1.598 900 68
K_3	−0.018 442 33			
L_3	1.999 842 70			
M_3	2.100 114 10			

[a]See Table S1 in the Supporting Information for the description of the parameters.

hydrogen vector $\mathbf{R}_{O0H_j}$ onto the donor-potential acceptor vector $\mathbf{R}_{O0O1_i}$. The ratio ρ_{ji} is defined as follows:

$$\rho_{ji} = \begin{cases} \dfrac{|\mathbf{R}_{O0H_j}^{//i}|}{|\mathbf{R}_{O0O1_i}|} & \text{if } \mathbf{R}_{O0H_j}^{//i} \cdot \mathbf{R}_{O0O1_i} > 0 \\ 0 & \text{otherwise} \end{cases} \quad (3)$$

The ratio ρ_{ji} is a measure of how likely H_j is going to be transferred to $O1_i$ (the larger positive the ρ_{ji} value, the more likely the transfer will be). At any given time step during the simulation, O1 is identified as the potential acceptor with the largest ρ_{ji} value, which is labeled as ρ. The donor and acceptor are swapped if $\rho > 0.5$. Please note that O1 is not necessarily the potential acceptor that is the closest to the donor O0, which is labeled as O1′, although O1 and O1′ are identical most of the time (>97%) during our MD simulations. Figure 4B shows a snapshot taken from an OM3*n* trajectory where O1 and O1′ have different identities. In this case, the acceptor O1 is further away from O0 than the nearest potential acceptor O1′, but the geometry clearly favors the proton transfer between O0 and O1.

Because of the large number of atoms in the above cluster models, it is computationally quite expensive to simulate the entire system even at the semiempirical level. We thus carried out the MD simulations at the combined quantum-mechanics/molecular-mechanics (QM/MM)[66−73] level. The inner core was described by semiempirical quantum chemistry, and the outer layer by the SPC[74] water potential. For the sake of simplicity, the mechanical embedding scheme[75] was adopted. Both the authentic and reparameterized semiempirical models were applied to the simulations of the charge-neutral water system, but only the reparameterized models were employed for simulating the hydrated proton. In the OM2 and OM2*n* simulations, we encountered self-consistent-field (SCF) convergence problems quite often, so we decided not to pursue them further; hence, we do not present OM2 and OM2*n* results for the bulk systems. The MD simulations were performed using the QMMM[76] program, which calls the MNDO[63] program for QM calculations and TINKER[77] for MM calculations. They were carried out in the canonical (*NVT*) ensemble at a temperature of 298.15 K, using a Nosé-Hoover thermostat.[78,79] For a given semiempirical model, 10 trajectories were propagated independently with a step size of 1 fs, each consisting of 2 ps equilibration followed by a 20 ps productive run. The total time length of the productive trajectories was 200 ps for each semiempirical model. For the bulk water simulations, the geometry of the entire system was saved every 50 steps. In the hydrated proton case, the geometry was saved every 10 steps, and the information about the donor and potential acceptors was recorded every step.

To limit the boundary effects due to the finite size of the model systems, the radial distribution functions (RDFs) for the water molecules were computed for an "elite" group of selected water molecules, more specifically, the 21 water molecules that were initially located within 5 Å from the center of the cluster. If an elite water molecule drifted away from the center of mass of the entire system by more than 5 Å at a given time step, the saved geometry of that snapshot was excluded from the corresponding RDF analysis. This RDF analysis procedure was first tested in two calculations at the MM level, where the entire system was described by the SPC[74] and TIP3P[80] water potentials, respectively. In either test, the RDF computed for the above cluster model was compared with the RDF obtained from 200 ps *NVT* simulations at the same temperature using periodic boundary conditions (PBC) with 216 water molecules in a cubic box of 18.63 Å length. Inspection of the cluster model-based RDF and the PBC-based RDF (see Figures S1 and S2 in the Supporting Information) revealed only minor and insignificant differences, which suggests that our approach is sufficiently accurate. For the RDF calculations of the hydrated proton, the criterion to include a snapshot was that the

dx.doi.org/10.1021/ct400224n | J. Chem. Theory Comput. 2013, 9, 2672−2686

Table 2. Parameters Re-optimized in This Work for the Orthogonalization-Corrected Models OM1, OM2, and OM3[a]

	OM1		OM2		OM3	
parameter	H	O	H	O	H	O
U_{ss} (eV)	−12.838 184 53	−93.042 206 09	−12.560 935 10	−101.852 535 97	−12.484 287 97	−105.829 748 09
U_{pp} (eV)		−77.598 439 87		−79.043 912 84		−78.874 514 70
ζ (au)	1.209 193 33	1.102 381 11	1.558 958 16	1.396 722 13	1.285 158 34	1.313 975 69
β_s (eV bohr$^{-1/2}$)	−4.892 972 58	−6.222 354 84	−3.313 643 01	−10.761 940 01	−3.358 940 34	−14.461 600 14
β_p (eV bohr$^{-1/2}$)		−9.940 330 68		−8.570 870 01		−8.741 752 81
β_π (eV bohr$^{-1/2}$)		−11.293 709 59		−9.434 719 22		−12.911 417 67
β_s(X−H) (eV bohr$^{-1/2}$)		−6.459 788 22		−6.640 584 53		−13.583 127 26
β_p(X−H) (eV bohr$^{-1/2}$)		−12.474 169 74		−10.192 763 80		−9.409 924 53
α_s (au)	0.096 316 41	0.108 573 45	0.098 526 80	0.111 786 91	0.060 830 99	0.084 727 80
α_p (au)		0.096 425 42		0.085 136 94		0.078 303 72
α_π (au)		0.152 820 61		0.166 179 91		0.143 615 89
α_s(X−H) (au)		0.079 434 49		0.075 948 50		0.173 009 39
α_p(X−H) (au)		0.129 291 89		0.083 188 46		0.117 783 94
G_{ss} (eV)	12.847 829 62	15.420 763 38	12.803 449 02	15.385 277 00	12.845 336 07	15.369 303 75
G_{pp} (eV)		14.520 494 26		14.547 376 40		14.578 254 22
G_{sp} (eV)		14.480 064 08		14.512 376 78		14.445 520 26
G_{p^2} (eV)		12.980 302 07		12.867 807 46		13.015 101 93
H_{sp} (eV)		3.940 777 43		3.992 884 32		3.950 34628
F_1	0.541 034 13	0.681 430 71	0.389 765 28	1.156 680 58	0.349 155 26	0.535 902 15
F_2	0.846 677 03	0.476 399 46	1.527 086 00	1.089 211 84		
G_1			0.660 531 90	0.262 691 92	0.333 525 83	0.052 674 67
G_2			0.915 091 13	0.869 410 78		

[a]See Table S1 in the Supporting Information for the description of the parameters.

hydronium O atom must be within 5 Å of the center of the cluster; it turned out that all saved snapshots satisfied this requirement and could be used. The integrated coordination number (ICN) for two types of atoms A and B: $n_{AB}(r) = 4\pi\int_0^r g_{AB}(r')r'^2\,dr'$ was computed in a similar way. Again, as can be seen from Figures S16(A) and S17(A) in the Supporting Information, we have obtained essentially identical plots of the oxygen−oxygen ICN $n_{OO}(r)$ and the oxygen−hydrogen ICN $n_{OH}(r)$ for water molecules in the simulations with PBC and with cluster models.

In this work, the nuclear degrees of freedom were treated classically. Therefore, quantum effects on the nuclear motion were not included. The zero-point vibrational corrections would effectively lower the free-energy barrier for proton transfer, but the change is known to be small (∼0.5 kcal/mol),[1] smaller than the root-mean-square deviation (RMSD) between the potential energy surfaces from the semiempirical and ab initio calculations. Tunneling effects are insignificant for proton transfer in bulk water,[1,17] as expected from the low free-energy barriers. Therefore, a classical treatment of nuclear motion was considered adequate for our purposes.

3. RESULTS AND DISCUSSION

3.A. Parameters. The OM*x* Hamiltonian differs from the MNDO-type Hamiltonian used in AM1 and PM3 by including orthogonalization corrections that account for Pauli exchange repulsions.[81] These corrections are applied to the one-center Fock matrix elements in OM1, and to all Fock matrix elements in OM2 and OM3. The corrections in OM2 are truncated in OM3 for computational efficiency without losing much of the accuracy. Moreover, while AM1 and PM3 attempt to use flexible core repulsion functions to model the interactions in weakly bound systems, the OM*x* methods put emphasis on the fine-tuning of the resonance integrals that represent the major bonding interactions. The optimized new parameters for hydrogen and oxygen are tabulated in Table 1 for the MNDO-based methods AM1 and PM3, and in Table 2 for the OM*x* models. A brief description of these parameters is given in Table S1 in the Supporting Information. The new values of the parameters are generally quite close to the original values: the maximum relative changes are <8% for AM1*n*, PM3*n*, and OM1*n*, and they mostly remain below 10% for OM2*n* and OM3*n* (except for a few larger changes in the parameters entering the resonance integrals and the prefactors of the orthogonalization terms). Therefore, the reparameterization should be regarded as a fine tuning of the investigated semiempirical methods (rather than a drastic modification).

3.B. Training and Validation Sets. The overall performance of the authentic parameters is documented in Table 3 by the RMSDs of the energies, geometries, and vibrational frequencies for the training set, using the ab initio results as the reference. We are particularly interested in the cluster binding energy (V), the two-dimensional potential surface for proton transfer (V^{PES}), and the hydrogen-bonding angle (θ_H) (which is important because it indicates the orientation of the water molecules in the hydrogen-bonding network). Obviously, the orthogonalization-corrected models outperform the MNDO-based methods in nearly all aspects. While the OM*x* models reproduce the reference data for the cluster binding energies V within 6 kcal/mol, the MNDO-based methods yield significantly larger errors ranging from 12 kcal/mol to 33 kcal/mol. A similar performance is observed for V^{PES}. In the case of θ_H, AM1 and PM6 show very large deviations (RMSDs of 48° and 33°, respectively), implying an erroneous orientation of the water molecules in the hydrogen-bonding network. OM1 (RMSD = 21°) and PM3 (RMSD = 13°) perform somewhat better, although not satisfactorily. The OM2 and OM3 results are best (RMSD < 5°). To exemplify the significance of θ_H, we superimpose the reference MP2 geometry for the Eigen cation with those obtained from different semiempirical methods in

Table 3. Root-Mean-Square Deviations (RMSDs) of the Standard Semiempirical Methods for the Training Set[a]

	MNDO-based			Orthogonalization-corrected		
	AM1	PM3	PM6	OM1	OM2	OM3
V (kcal/mol)	12.5	32.5	16.6	5.5	5.8	4.1
r (Å)	0.01	0.01	0.03	0.01	0.01	0.05
r_H (Å)	0.36	0.15	0.10	0.22	0.15	0.23
θ (deg)	3.6	2.9	7.0	1.6	2.2	1.5
θ_H (deg)	47.6	13.1	32.8	20.9	4.6	4.2
$\nu(cm^{-1})^b$	235	204	695	116	372	229
$n_{i\nu}$	3	1	1	3	1	1
V^{PES} (kcal/mol)	19.7	39.2	15.8	3.9	8.5	5.4

[a]The training set consists of 7 potential energies (V), 35 bond lengths (r), 11 hydrogen-bond lengths (r_H), 22 bond angles (θ), 16 hydrogen-bond angles (θ_H), 114 frequencies (ν), and the number of imaginary frequencies ($n_{i\nu}$) in the water clusters and charged water clusters [model systems (a)−(g) in Figure 1]. It also includes 53 data points of the two-dimensional potential energy surface (V^{PES}) for proton transfer in the Zundel ion at fixed R_{OO} distances (see Figure 2A). See Section 2 for computational details. [b]The total number of reference frequencies is 114; any imaginary frequencies are excluded from the statistics.

Table 4. Root-Mean-Square Deviations (RMSD) of the Reparameterized Semiempirical Methods for the Training and Validation Sets[a]

	MNDO-based		Orthogonalization-corrected		
	AM1n	PM3n	OM1n	OM2n	OM3n
	Training Set[b]				
V (kcal/mol)	11.6	7.4	5.1	0.5	2.0
r (Å)	0.01	0.01	0.01	0.01	0.02
r_H (Å)	0.36	0.38	0.21	0.04	0.04
θ (deg)	3.7	3.8	1.5	0.9	1.3
θ_H (deg)	47.4	15.4	13.6	2.8	4.1
ν $(cm^{-1})^c$	243	145	119	383	245
n_ν	4	3	5	2	2
V^{PES} (kcal/mol)	18.4	1.0	3.9	0.5	0.7
	Validation Set[d]				
V (kcal/mol)	7.1	8.3	13.5	0.2	1.6
r (Å)	0.02	0.01	0.02	0.01	0.02
r_H (Å)	0.66	0.11	0.41	0.02	0.01
θ (deg)	2.1	1.3	2.8	0.7	0.4
θ_H (deg)	83.7	3.7	49.7	7.3	6.4
V^{PES} (kcal/mol)	19.3	0.9	3.3	0.8	0.6

[a]See Section 2 for computational details. [b]See footnote (a) of Table 3. [c]See footnote (b) of Table 3. [d]The validation set consists of 3 potential energies (V), 26 bond lengths (r), 13 hydrogen-bond lengths (r_H), 13 bond angles (θ), 12 hydrogen-bond angles (θ_H) of the water clusters and charged water clusters (model systems (h)−(j) in Figure 1). It also includes 46 data points of the two-dimensional potential energy surface (V^{PES}) for proton transfer in the Zundel ion at fixed R_{OO} distances (see Figure 2B).

Figure S3 of the Supporting Information. The MP2 calculations yield θ_H = 175.2°. The MNDO-based methods, AM1 (θ_H = 100.7°), PM3 (θ_H = 150.2°), and PM6 (θ_H = 136.7°), produce qualitatively wrong orientations of the coordinating water molecules with respect to the central hydronium ion, whereas the OMx methods predict much more realistic angles θ_H of 172.9°, 168.9°, and 175.0° for OM1, OM2, and OM3, respectively.

How do the reparameterized methods perform? First, we look at the training set (rows 4−11 of Table 4). The reparameterization leads to substantial improvements in the energies for PM3n, OM2n, and OM3n, but only slight changes for AM1n or OM1n. The most impressive advances are observed for PM3n. Overall, OM2n and OM3n clearly show the best performance, achieving excellent agreement with the ab initio reference data for V (RMSD = 0.5 and 2.0 kcal/mol, respectively) and V^{PES} (RMSD = 0.5 and 0.7 kcal/mol, respectively). In terms of the hydrogen-binding geometries, OM2n and OM3n are again superior with small RMSD values for θ_H (2.8° and 4.1°, respectively). Again using the Eigen cation as an example (see Figure S3 in the Supporting Information), AM1n still gives an erroneous hydrogen bonding angle (θ_H = 101.8°), the PM3n value (θ_H = 167.4°) underestimates the MP2 value by 7.8°, and the reparameterized OMx models reproduce the MP2 angle within 2.6°.

Next, we turn to the validation set (see rows 13−18 in Table 4; optimized geometries for entries (h)−(j) are given in Figures S4−S6 in the Supporting Information). Overall, each of the reparameterized semiempirical models shows a rather similar performance for the validation set and the training set. However, two exceptions should be noted. First, PM3n achieves a very small RMSD value for θ_H (3.7°), indicating excellent hydrogen-bonding geometries in the validation set. Second, OM1n gives much larger RMSD values for V and θ_H due to poor geometries for the water tetramer and pentamer, which maintain the cyclic structure, but adopt hydrogen-bond orientations that deviate substantially from the MP2 geometry. The OM1n geometry for the Zundel ion complex with two water molecules is still in good agreement with the ab initio result.

Finally, we take a look at the two-dimensional (2D) potential surfaces for proton transfer within a Zundel ion in the gas phase computed by the reparameterized methods (Figure 5). The reference MP2 surface clearly shows a well at (R_{OO}, dr) ≈ (2.4 Å, 0), which corresponds to the symmetric Zundel ion. Here, dr is the difference in the distances from the migrating proton to either O atom. The AM1n surface differs from the reference MP2 surface significantly, displaying a well in the upper right corner that is deeper than the central well of the symmetric Zundel ion; this suggests that the lowest-energy AM1n structure of the Zundel ion is very asymmetric (also see Figure S5(B) in the Supporting Information), and should perhaps better be regarded as a water molecule that is hydrogen-bonded to a hydronium ion. Because hydrogen moves much faster than oxygen, due to the much smaller mass, proton transfers can be approximated by movements along vertical lines on the two-dimensional surfaces shown in Figure 5. Since the asymmetric AM1n well is located at $R_{OO} \geq$ 2.8 Å, the barrier for proton transfer will be quite high (>6 kcal/mol). The PM3n surface shows a narrow valley extending from (R_{OO}, dr) ≈ (2.36 Å, 0) to (R_{OO}, dr) ≈ (2.44 Å, 0.3 Å). Such a surface is not optimal for proton transfer, although the RMSD value in V^{PES} is rather small (<1 kcal/mol). By contrast, all OMxn surfaces resemble the reference MP2 surface in giving a central well for the symmetric Zundel ion. The OM2n surface seems to agree best with the MP2 surface, followed by the OM3n surface; both show a central well near (R_{OO}, dr) ≈ (2.41 Å, 0). The OM1n surface has a central well that is somewhat displaced at (R_{OO}, dr) ≈ (2.34 Å, 0). Interestingly, the OM3n surface, and to a slightly lesser extent also the OM2n surface, resemble the

dx.doi.org/10.1021/ct400224n | J. Chem. Theory Comput. 2013, 9, 2672−2686

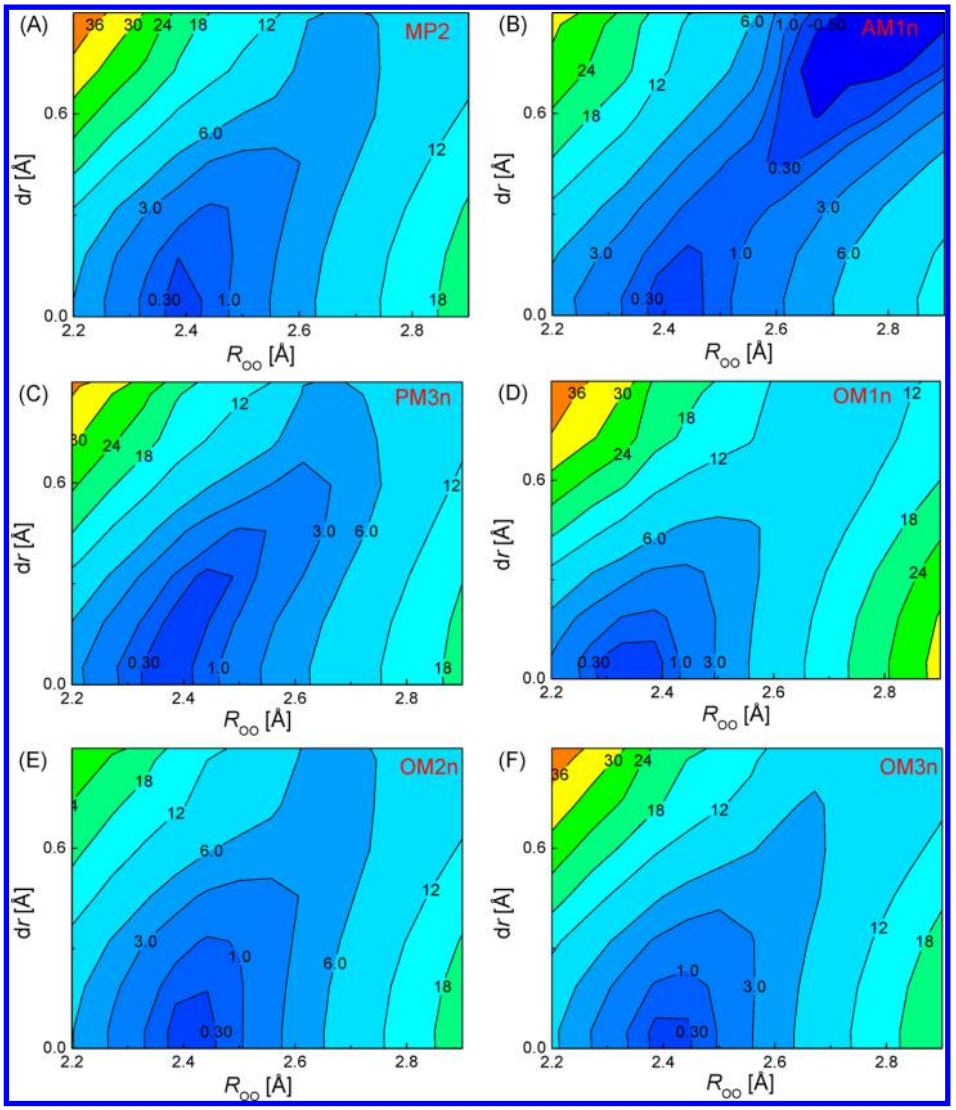

Figure 5. Two-dimensional gas-phase energy surfaces for proton transfer in the Zundel ion at fixed distances R_{OO} (in Ångstroms) obtained from (A) MP2/aug-cc-pVTZ and (B–F) the reparameterized semiempirical methods. Here, d*r* is the difference in the distances between the migrating proton and the two O atoms.

effective ab initio path-integral surface for the Zundel ion calculated by Brancato and Tuckerman (see Figure 1B in ref 21), who have parametrized an MS-EVB model on the basis of the path-integral surface, so that quantum effects such as the zero-point energy are implicitly included.

3.C. Binding Energy Profile of the Water Dimer. The gas-phase binding energy curves of the water dimer are plotted in Figure 6. Panel (A) shows those computed with the authentic parameters. First, we note that, at short distances R_{OO}, all methods including MP2 experience difficulties in getting smooth curves, because of changes in the relative orientation of the water molecules. Taking MP2 as an example, at $R_{OO} \geq 2.6$ Å, the first water molecule lies in a plane that bisects the HOH angle of the second water molecule, whereas at $R_{OO} \leq 2.5$ Å, both molecules are in the same plane (Figure S12 in the Supporting Information). This change in relative orientation only gives rise to a small bump in the MP2 energy profile, but leads to larger kinks in the curves computed semiempirically. Second, we note that all semiempirical methods except AM1 predict water dimers that are underbound, and the optimal distances between the two O atoms are shorter than the MP2 value. At large distances R_{OO}, all semiempirical models, including AM1, underestimate the binding energy, presumably because of the lack of explicit dispersion terms. Interestingly, the OM*x* curves seem to converge faster to the MP2 curve than the MNDO-based curves do when the water molecules are gradually taken apart. Adding empirical dispersion corrections may help to improve the agreement at large distances.[54,82,83] However, dispersion interactions were not deemed to be the main problem in the parametrization of the energy surface for proton transfer, where the two water molecules within the Zundel ion are in close proximity, so that electrostatic interactions are expected to be dominant. Therefore, we have not included empirical dispersion corrections in this work.

The energy profiles computed with the reparameterized methods are depicted in panel (B) in Figure 6. While the AM1*n* curve has changed little from AM1, the PM3*n* curve has changed remarkably from PM3. The binding well around R_{OO} = 2.8 Å in PM3 moves to R_{OO} = 3.1 Å in PM3*n*, and moreover becomes very shallow, with the binding energy decreased from 4 kcal/mol to 2 kcal/mol. The OM1*n* curve looks very similar

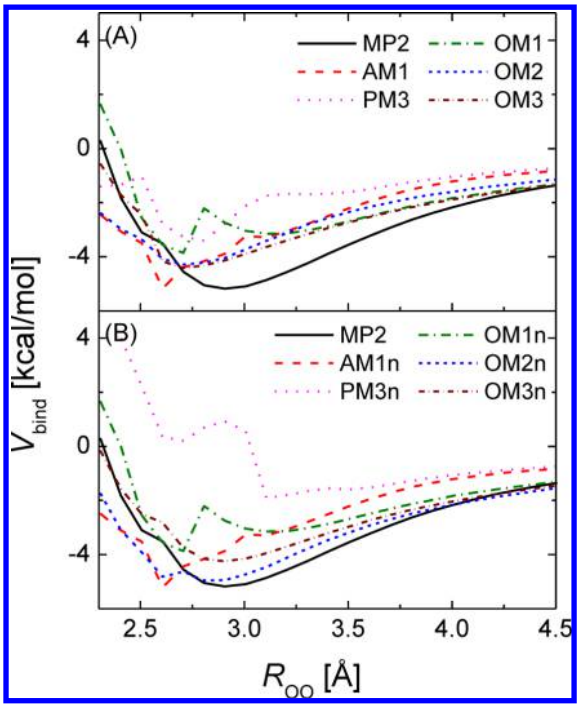

Figure 6. Gas-phase binding energy profiles of two water molecules computed with the (A) authentic and (B) reparameterized semi-empirical methods. The solid reference curve was obtained at the MP2/aug-cc-pVTZ level from relaxed surface scans for the water dimer as a function of distance between the two O atoms (R_{OO}), in steps of 0.1 Å. The zero of energy corresponds to two water molecules at infinite distance: $V_{bind} = V_{(H_2O)_2} - 2V_{H_2O}$.

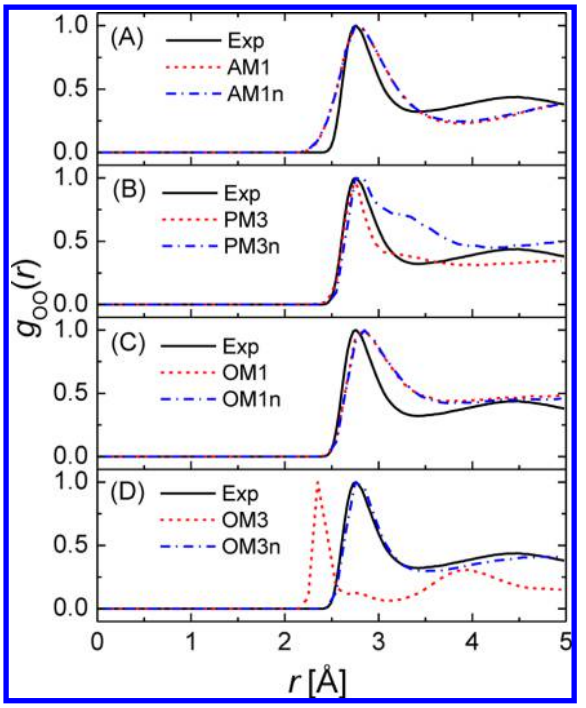

Figure 7. Radial distribution functions $g_{OO}(r)$ for water computed for (A) AM1 and AM1*n*, (B) PM3 and PM3*n*, (C) OM1 and OM1*n*, and (D) OM3 and OM3*n*. The experimental data (denoted by "Exp") is plotted in all panels for comparison. The AM1 and OM1 curves are directly beneath the AM1*n* and OM1*n* curves, respectively. All curves have been scaled such that the height of the first peak is 1.00.

to the OM1 curve. The OM2*n* curve shows the best agreement with the MP2 curve, followed by the OM3*n* curve. Compared with OM2 and OM3, the improvements in OM2*n* and OM3*n* are most encouraging at larger distances (R_{OO} > 2.8 Å), which further alleviates the need to include empirical dispersion corrections.

3.D. Properties of Water. The oxygen−oxygen and oxygen−hydrogen RDF obtained from the bulk water simulations are plotted in Figures 7 and 8, respectively, together with the experimental curves.[84,85] First, let us look at the oxygen−oxygen RDF. Both AM1 and AM1*n* give a first (broad) peak near r = 2.8 Å, but fail to predict the second peak at $r \approx 4.5$ Å; the minimum between the first and second peaks occurs at $r \approx 3.9$ Å, which is a larger distance than that found experimentally (r = 3.4 Å). The PM3 curve shows the first peak near r = 2.8 Å, with a small shoulder between r = 3.0 Å and r = 3.5 Å. In the PM3*n* curve, the shoulder becomes more prominent. Neither PM3 nor PM3*n* predict the second peak correctly. The OM1 and OM1*n* RDF are similar, with the first peak at r = 2.9 Å and the second peaks not seen. The OM3 curve has a first sharp peak at a distance that is much too short (r = 2.4 Å), but the reparameterization improves the RDF dramatically: the OM3*n* curve shows the best agreement with the experimental RDF, although the second peak is still slightly off (by <0.3 Å). The difficulties in reproducing the second peak with AM1, PM3, and OM1 (and their reparameterized counterparts) are likely due to the problem that they all underestimate the binding energies between water molecules (see Figure 6).

The first-solvation-shell coordination numbers were estimated by $n_{OO}(r)$ at the r values that correspond to the first

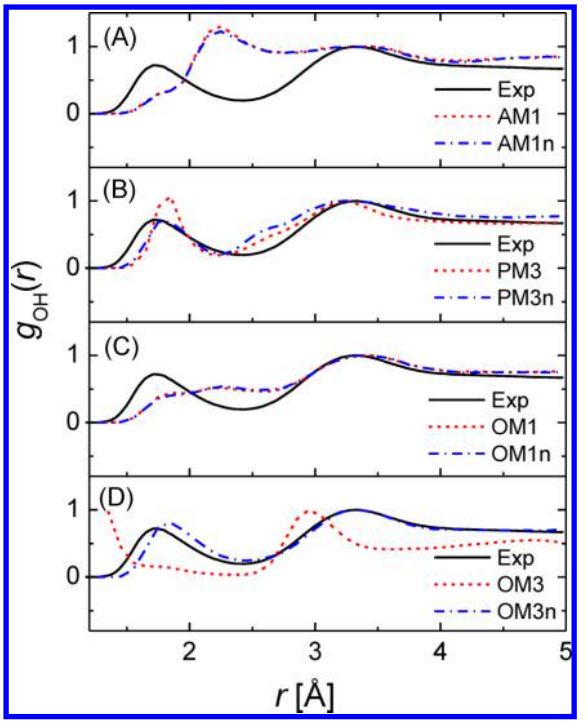

Figure 8. Radial distribution functions $g_{OH}(r)$ for water computed for (A) AM1 and AM1*n*, (B) PM3 and PM3*n*, (C) OM1 and OM1*n*, and (D) OM3 and OM3*n*. The experimental data (denoted by "Exp") is plotted in all panels for comparison. The AM1 and OM1 curves are right beneath the AM1*n* and OM1*n* curves, respectively. All curves have been scaled such that the height of the peak at ~3 Å is 1.00.

dx.doi.org/10.1021/ct400224n | J. Chem. Theory Comput. 2013, 9, 2672−2686

minima of $g_{OO}(r)$, and the results echo the above RDF analysis. The first-solvation-shell coordination numbers are tabulated in the second column of Table 5, and the $n_{OO}(r)$ plots are given in

Table 5. Integrated Coordination Numbers of the First Solvation Shell for Water and for Hydronium from Semiempirical MD Simulations[a]

	Integrated Coordination Number, ICN	
	water[b]	hydronium[c]
AM1	8.7	n/a
AM1*n*	9.4	10.4
PM3	8.0	n/a
PM3*n*	7.7	7.9[d]
OM1	6.4	n/a
OM1*n*	6.7	7.8[e]
OM3	3.7	n/a
OM3*n*	4.9	6.5

[a]ICNs at the distances corresponding to the first minima in $g_{OO}(r)$ for water and in $g_{OOO}(r)$ for hydronium, unless otherwise indicated. [b]4.7 in the experiments[84−86] and 4.1 in ab initio MD simulations.[37] [c]3.0 in ab initio MD simulations.[37] [d]Including the peak at r = 3.0 Å (otherwise, ICN = 3.3). [e]Integration over both peaks in the bimodal distribution.

panels (B) and (C) of Figure S16 in the Supporting Information. Compared with the coordination number value of 4.7 determined experimentally,[84−86] it is apparent that the MNDO-based methods overestimate the number of coordinating water molecules due to the erroneous hydrogen-bonding pattern. Better performance is achieved by the orthogonalization-corrected methods, because of their improved hydrogen-bonding description. In particular, OM3*n* yields a coordination number of 4.9 that is in excellent agreement with the experiments.

Turning to the oxygen−hydrogen RDF, we find that none of original semiempirical methods with authentic parameters reproduces the experimental curve correctly. PM3 performs best, predicting two peaks at r = 1.9 Å and 3.3 Å that are rather close to the experimental ones at r = 1.7 Å and 3.3 Å, respectively; however, the first PM3 peak is much too narrow. Reparameterization again leads to dramatic improvements in the OM3 case: the OM3*n* RDF matches the experimental curve very well, although the position of the first peak deviates slightly, by ∼0.1 Å. There are also improvements in the PM3 case, leading to lower and broader peaks in the PM3n curve, but the agreement is not as good as for OM3*n*. The AM1 and OM1 RDF are not affected much by the reparameterization. Taken together, the above results clearly show that OM3*n* offers the best structural properties for bulk water.

3.E. Structural Properties of the Hydrated Proton. The RDF for water O atoms around the hydronium O atom (O0) are plotted in Figure 9. A bimodal distribution is found with OM1*n*: a narrower peak near r = 2.4 Å and a wider peak at $r \approx$ 2.6 Å. Maupin et al.[37] observed similar bimodal distributions in their SCC-DFTB simulations and interpreted them in terms of a prominent Zundel character for the solvated proton, with one of the three coordinating water molecules sustainably closer to the hydronium ion than the other two. Indeed, integration over the first peak in our OM1*n* plot yielded a coordination number of 1.4. This bimodal distribution is not seen in experiments or ab initio MD simulations. The recently reparameterized SCC-DFTB model by Cui and co-workers[39] gave a better overlap between the distributions of the three coordinating water O

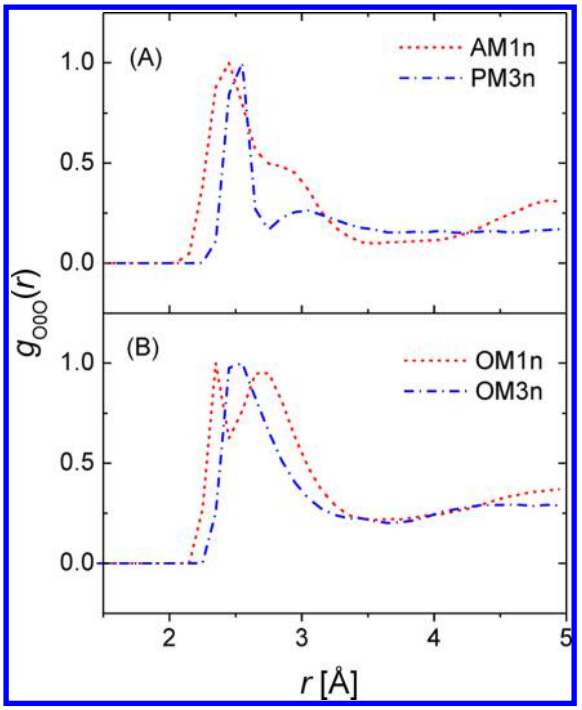

Figure 9. Radial distribution functions $g_{OOO}(r)$ for an excess proton in water computed with the reparameterized semiempirical methods; O0 represents the hydronium O atom. All curves have been scaled such that the height of the first peak at $r \approx$ 2.5 Å is 1.00.

atoms, which removed the bimodal distribution. Our OM3*n* model also predicts a single peak near r = 2.5 Å, in good agreement with the experiment and ab initio MD simulations. The AM1*n* RDF displays a single peak at r = 2.5 Å, with a shoulder near r = 2.9 Å. This shoulder becomes another lower and wider peak at $r \approx$ 3.0 Å in the PM3*n* curve.

The first-solvation-shell coordination numbers are given in the third column of Table 5. Compared with the coordination number of 3.0 from the ab initio MD simulations,[37] all coordination numbers from the semiempirical methods in Table 5 are much larger, including the OM3*n* result (6.5). We note that previous SCC-DFTB simulations[37,39] produced coordination numbers in the range of 4.5−5.2, which are closer to, but still larger than, the ab initio MD value. The larger coordination numbers in the semiempirical simulations indicate more fluidic structures around the hydronium ion, as also implied by the less-prominent second peaks and the minima at larger r values in the $g_{OO}(r)$ curves.

The RDF for hydrogen atoms around O0 is displayed in Figure 10. The first peak at ∼1 Å is due to the covalently bound H atoms in the hydronium ion. Near r = 1.8 Å, a small peak can be found in the PM3*n*, OM1*n*, and OM3*n* curves. This peak is caused by the H atom of the water molecule that is hydrogen-bonding to the hydronium ion oxygen. AM1*n* does not yield this small peak, because it does not properly describe the hydrogen-bonding network (see the earlier discussion on the hydrogen-bonding angles). All reparameterized models successfully predict the peak at 3.1 Å. On the basis of this evidence (Figures 9 and 10), we conclude that it is again OM3*n* which best reproduces the structural properties.

Traditionally, the structures of the solvated proton are classified as Eigen- or Zundel-like. However, the distinction between distorted Eigen and distorted Zundel structures is not clear-cut. There are various ways to define the Eigen-like and

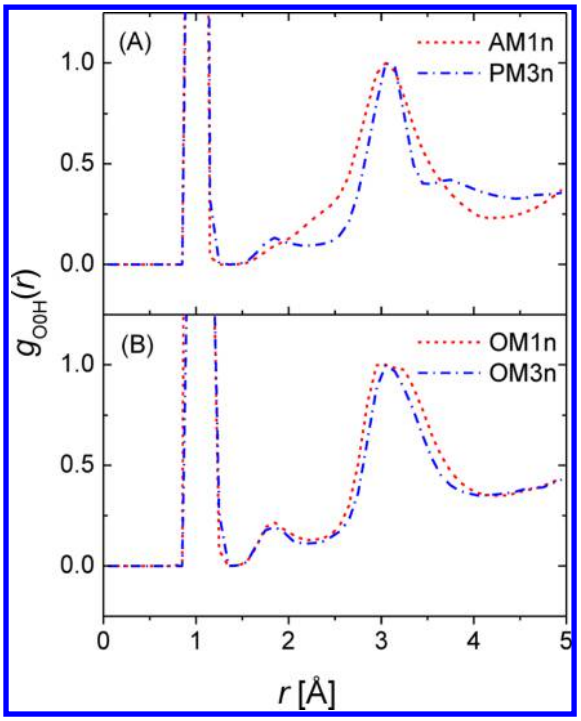

Figure 10. Radial distribution functions $g_{O0H}(r)$ for an excess proton in water computed with the reparameterized semiempirical methods; O0 represents the hydronium O atom. All curves have been scaled such that the height of the peak at $r \approx 3.0$ Å is 1.00.

Zundel-like geometries.[17,27,36,37] In this work, we tested three definitions based on different geometric parameters, the distributions of which are illustrated by histograms in Figure S13 in the Supporting Information. The first definition (Def-1) used by Choi and Jordan[36] employs the distance between the hydronium oxygen O0 and the oxygen of the nearest potential acceptor O1′ ($R_{O0O1'}$) as the criterion: Zundel for $R_{O0O1'} < 2.46$ Å, intermediate for 2.46 Å $\leq R_{O0O1'} \leq 2.49$ Å, and Eigen for 2.49 Å $< R_{O0O1'}$. The second definition (Def-2) is similar to that used by Marx et al.[27] and relies on the position of H′, the hydrogen located between O0 and O1′; here, the criterion is the distance difference $dr = |R_{O0H'} - R_{O1'H'}|$: Zundel for $dr <$ 0.1 Å, intermediate for 0.1 Å $\leq dr \leq$ 0.2 Å, and Eigen for 0.2 Å $< dr$, where $R_{O0H'}$ and $R_{O1'H'}$ denote the distances between O0 and H′ and between O1′ and H′, respectively; the currently chosen Eigen dr value of 0.2 Å (instead of 0.3 Å in ref 33) has been suggested by Markovitch et al.[17] The third definition (Def-3) is based on the ratio ρ (see Figure 4): Zundel for $\rho >$ 0.46, intermediate for 0.45 $\leq \rho \leq$ 0.46 Å, and Eigen for $\rho <$ 0.45. We adopted ρ values of 0.45 and 0.46 Å for the following reason. The MP2-optimized Eigen structure has $R_{O0O1} = 2.554$ Å and $R_{O0H} = 1.011$ Å. To reduce the noise from the fast OH stretching vibrations of the hydronium ion, we (arbitrarily) took $R_{O0H} = 1.05$ Å as the starting point of proton transfer, which gave $\rho_{start} = 0.41$; we note that the value of 1.05 Å is close to the average O0H bond length of 1.057 Å from ab initio path integral calculations.[21,27] Because of the donor–acceptor swap at $\rho_{end} = 0.5$, we chose $\rho_{mid} = 0.455$ (with 0.005 at each side as the intermediate buffer) to be the boundary separating Eigen and Zundel. The average values of the relevant geometric parameters and the percentages of the Eigen, intermediate, and Zundel structures for the saved trajectories are listed in rows 6–17 of Table 6.

Table 6. Statistics of the Observed Donor–Acceptor Swaps, Grotthuss Shuttling Rates (Forward Hop), and Zundel-Eigen Structural Classifications for the Trajectories Obtained with the Reparameterized Semiempirical Methods[a]

	AM1*n*	PM3*n*	OM1*n*	OM3*n*
number of swaps	0	306	9364	4678
average time between swaps	n/a	0.65 ps	0.02 ps	0.04 ps
forward hops	0	11	91	105
average time between forward hops	n/a	18 ps	2.2 ps	1.9 ps
Def-1				
$\langle R_{O0O1'} \rangle$	2.31 Å	2.46 Å	2.35 Å	2.44 Å
Zundel	97.7%	51.2%	96.9%	64.0%
Eigen	0.8%	24.9%	1.3%	18.1%
Intermediate	1.5%	23.9%	1.8%	17.9%
Def-2				
$\langle dr = \lvert R_{O0H'} - R_{O1'H'} \rvert \rangle$	1.03 Å	0.45 Å	0.19 Å	0.28 Å
Zundel	0	1.4%	36.1%	19.6%
Eigen	100.0%	96.4%	35.6%	59.3%
Intermediate	0	2.2%	28.4%	21.1%
Def-3				
$\langle \rho \rangle$	0.309	0.416	0.464	0.453
Zundel	0	3.4%	61.9%	41.4%
Eigen	100.0%	94.6%	27.4%	46.5%
Intermediate	0	2.0%	10.7%	12.1%

[a]Based on 10 trajectories for each semiempirical model, each consisting of 2 ps equilibration and a 20 ps productive run. The criterion for donor–acceptor swaps is illustrated in Figure 4. The forward hop rate is defined in eqs 4 and 5 of the text. Three ways to define Zundel and Eigen structures have been used here. Def-1 is based on $R_{O0O1'}$: Zundel for $R_{O0O1'} < 2.46$ Å, intermediate for 2.46 Å $\leq R_{O0O1'} \leq 2.49$ Å, and Eigen for 2.49 Å $< R_{O0O1'}$. Def-2 is based on $dr = |R_{O0H'} - R_{O1'H'}|$: Zundel for $dr <$ 0.1 Å, intermediate for 0.1 Å $\leq dr \leq$ 0.2 Å, and Eigen for 0.2 Å $< dr$. Def.-3 is based on ρ (see Figure 4): Zundel for $\rho > 0.46$, Intermediate for 0.45 $\leq \rho \leq$ 0.46 Å, and Eigen for $\rho <$ 0.45. See Section 3.E for further discussion.

It is remarkable that these different definitions lead to rather different classifications of the geometries of the hydrated proton in the saved trajectories. While most of the geometries are characterized as Zundel-like by Def-1, the Eigen "flavor" is more prominent according to Def-2 and Def-3. Most noticeably, the AM1*n* geometries are considered almost exclusively Zundel-like by Def-1 but 100% Eigen-like by Def-2 and Def-3. The classifications by Def-2 and Def-3 are qualitatively similar, albeit with more geometries in the OM1*n* and OM3*n* trajectories being identified as distorted Eigen structures by Def-3. Such similarity is not surprising, because both Def-2 and Def-3 characterize the solvated proton structures by assessing how symmetrical the location of the migrating proton is. The AM1*n* and PM3*n* geometries appear to be very asymmetric on average, and, therefore, identifying them as being Eigen-dominated seems appropriate. Both OM1*n* and OM3*n* simulations yield mixed Zundel and Eigen structures in comparable amounts. However, the OM1*n* geometries are generally more symmetric than the OM3*n* geometries, implying that the Zundel population is higher in the OM1*n* simulations.

3.F. Dynamic Properties of Proton Transfer. Inspection of the trajectories revealed that no proton transfer ever occurred in the AM1*n* simulations. Proton transfer was observed occasionally in the PM3*n* simulations, and was

found more frequently in the OM1*n* and OM3*n* simulations. The average time intervals between the proton shuttling were 0.65, 0.02, and 0.04 ps for PM3*n*, OM1*n*, and OM3*n*, respectively (row 3 in Table 6). These time intervals do not distinguish between the fast subpicosecond back-and-forth proton exchange within a donor−acceptor pair of a Zundel structure and the true proton transfer that results in a localized distorted Eigen structure, the latter of which occurring at a longer time scale. Similar to what has been done previously,[16] we computed the Grotthuss shuttling rate, or the forward hop rate, using an accumulation function:

$$h(t) = h(t - \Delta t) + \Delta h(\Delta t)$$
$$h(0) = 0 \quad (4)$$

where Δt is the time step, and $\Delta h(\Delta t)$ is given by

$$\Delta h(\Delta t) = \begin{cases} 0 & \text{if no proton hops} \\ 0 & \text{if a proton hops back to the last donor} \\ 1 & \text{if a proton hops to a new donor} \end{cases} \quad (5)$$

Note that $\Delta h(\Delta t)$ is defined here in a different way than previously defined.[16] The average time intervals between forward hops are found to be 18, 2.2, and 1.9 ps for the PM3*n*, OM1*n*, and OM3*n* simulations, respectively (row 5 in Table 6), indicating corresponding average rates of proton hopping of 0.06, 0.45, and 0.53 ps^{-1}, respectively. Interestingly, although proton transfer occurs more frequently in the OM1*n* simulations, there are more successful Grotthuss shuttling events for OM3*n*. The OM1*n* and OM3*n* hopping rates are close to the estimated experimental effective hopping rate (0.71 ps^{-1})[16] and to the rates obtained in the SCC-DFTB (~0.5 ps^{-1}) and CPMD (0.4 ps^{-1}) simulations by Maupin et al.[37] For comparison, we note that MS-EVB simulations[16] yielded a rate of 0.16 ps^{-1}.

We next look at the potentials of mean force (PMF) for proton transfer shown in Figure 11, where both $dr = |R_{O0H'} - R_{O1'H'}|$ and ρ are employed as distinguished reaction coordinates. Both yield a qualitatively similar picture of proton transfer for any given semiempirical method. The PMF from PM3n clearly indicates that the resting Eigen state ($dr \approx 0.5$ Å or $\rho \approx 0.41$) is more stable than the transition Zundel state ($dr \approx 0$ or $\rho \approx 0.5$) by ~2 kcal/mol. The barrier is quite high, compared with the thermal energy at temperatures near 300 K ($k_BT \approx 0.6$ kcal/mol), so that there are only occasional proton hops in the PM3*n* simulations. The OM3*n* model also predicts the Eigen−Zundel−Eigen proton transfer mechanism but with much lower barriers: 0.06 kcal/mol in the dr plot and 0.19 kcal/mol in the ρ plot. These OM3*n* effective barriers are lower than the classical CPMD barriers of 0.5 kcal/mol,[27,37] but, incidentally, are very close to the 0.15 kcal/mol barrier from ab initio path integral calculations,[27,33] which include the quantum fluctuations of all nuclei. A very shallow OM3*n* minimum corresponding to the Eigen structure is found near $dr = 0.25$ Å, again in excellent agreement with the ab initio path integral calculations.[21,27,33] By contrast, the PMFs from OM1*n* yield minima at the Zundel structure and thus indicate a Zundel−Zundel mechanism, which is consistent with the results of Maupin et al. from standard SCC-DFTB and from a specially parametrized SCC-DFTB version with a hydrogen-bonding damping function.[37] Cui and co-workers[39] also found the Zundel−Zundel mechanism in their standard and hydrogen-bonding-corrected SCC-DFTB simulations, while their third-order SCC-DFTB model with hydrogen-bonding corrections and a modified O−H repulsion potential gave the Eigen−Zundel−Eigen mechanism (albeit with a rather-high 0.9 kcal/mol free-energy barrier for proton transfer).

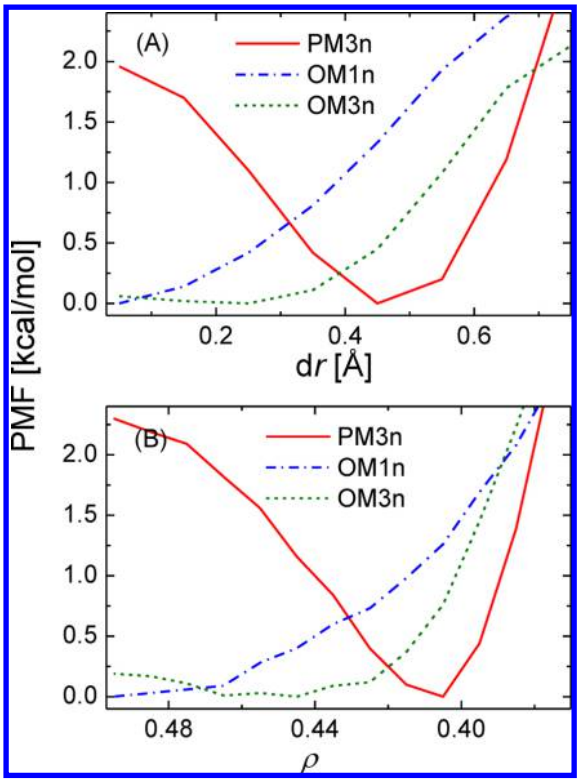

Figure 11. Potential of mean force (PMF) for the solvated proton: (A) The reaction coordinate is the distance difference $dr = |R_{O0H'} - R_{O1'H'}|$, where O0 is the hydronium oxygen atom, O1′ is the nearest potential acceptor, and H′ is the hydrogen between them ($R_{O0H'}$ ($R_{O1'H'}$) is the distance between O0 (O1′) and H′); (B) the reaction coordinate is the ratio ρ (see Figure 4 for definition).

Examples for the evolution of the hydronium O atom index in a representative sample trajectory are provided in Figure 12A for the PM3*n*, OM1*n*, and OM3*n* simulations. Also shown is the percentage of time when the given atom is identified as the hydronium-ion O atom. The sample trajectories were selected by requiring that the number of hydronium oxygen switches in the 20 ps trajectory should be approximately the same as the average number observed in all 10 trajectories for a given semiempirical model. In the PM3*n* sample trajectory, only two O atoms were ever identified as the donor, with O220 being the dominant one (>99% of the time). By contrast, five and four O atoms served as donor in the OM1*n* and OM3*n* sample trajectories, respectively, and in either case, three of these atoms were associated with the hydronium ion for a long time (>9%), which is consistent with the picture of frequent proton transfer previously discussed. For instance, in the OM3*n* sample trajectory, the donor switched from O529 to O109 shortly after the productive run began, remained at O109 for ~10 ps with many short visits to O55 and O394 of up to ~50 fs, and then migrated to O106 after a period of ~3 ps that featured many rapid rattles between O109 and O106. Such dynamics was found to be typical of the OM3*n* simulations. The forward hop rates $h(t)$ are plotted in Figure 12B for the sample trajectories. The flat plateaus represent the resting Eigen state of no proton transfer with oscillatory shuttling in the Zundel structure, while the often-clustered steps indicate Grotthuss

dx.doi.org/10.1021/ct400224n | J. Chem. Theory Comput. 2013, 9, 2672−2686

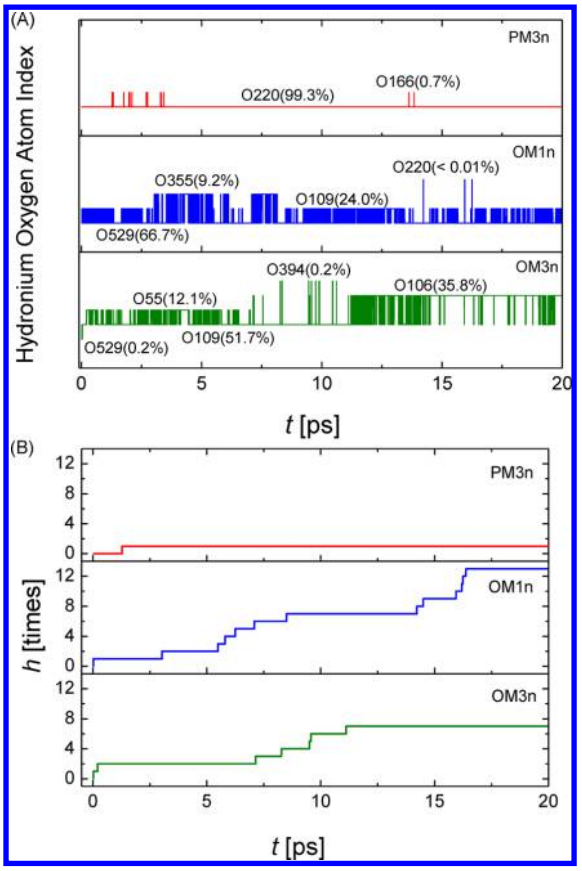

Figure 12. Evolution of (A) the hydronium O atom index and (B) the forward hop rate in sample trajectories from the PM3*n*, OM1*n*, and OM3*n* simulations. The percentage of time when the given atom was identified as the hydronium ion O atom is shown in panel (A) in parentheses. In the sample trajectories, the hydronium O atom index changed 30 times for PM3*n*, 1207 times for OM1*n*, and 576 times for OM3*n*. The average numbers of such changes in all trajectories are 31 for PM3n, 936 for OM1*n*, and 468 for OM3*n*. In panel (B), the forward hop rate $h(t)$ is defined in eqs 4 and 5 of the text. No donor−acceptor swapping occurred in the AM1 (AM1*n*) simulations.

proton transfer events. The length of the plateaus varies, but is roughly in the range of 5−10 ps for the OM1*n* and OM3*n* simulations (generally somewhat longer for OM3*n*). The length of the plateaus is determined by the fluctuation-induced breakage and reorganization of hydrogen bonds in the solvation shells, which are the rate-limiting steps of proton diffusion.[1,17]

Figure 13 displays the geometries of the sample trajectories projected onto the $R_{O0O1'}$−dr plane, as well as the corresponding gas-phase two-dimensional potential surfaces V^{PES} for proton transfer. While V^{PES} differs from the free-energy surface for proton transfer in bulk water, the plots are instructive in connecting the simulated trajectories with the potential surfaces used in the parametrization (see Section 3.B). As discussed previously, the gas-phase PM3*n* surface yields a narrow valley, which differs noticeably in shape from the reference MP2 surface. Here, we find that the PM3*n* sample trajectory spends the majority of time wandering in the area centered at $R_{O0O1'}$ = 2.45 Å and dr = 0.45 Å, roughly corresponding to one end of the narrow valley. Compared with the MP2 surface, the well in the OM1*n* surface is wider in the R_{OO} direction but narrower in the dr direction; this is consistent with the concentration of the OM1*n* geometries at small values of dr. The well in the OM3*n* surface resembles the

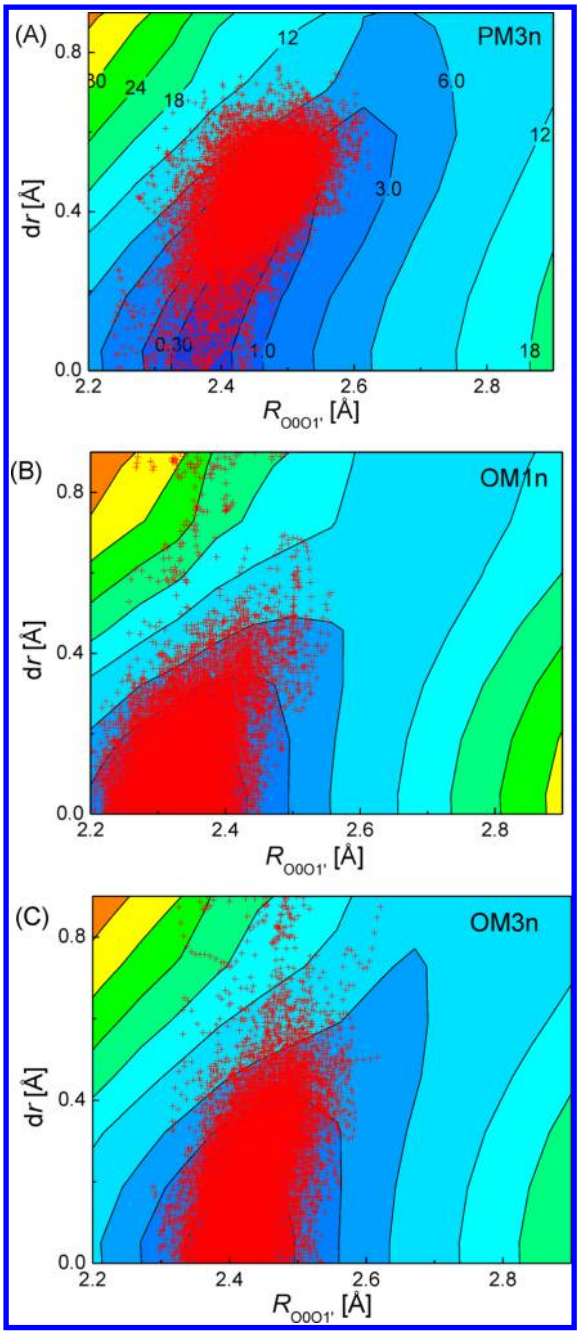

Figure 13. Projections of the geometries in the sample trajectories in Figure 11 for (A) PM3*n*, (B) OM1*n*, and (C) OM3*n*. The *x*-axis represents the distance between the hydronium oxygen O0 and the oxygen of the nearest potential acceptor O1′; the *y* axis represents the distance difference dr = $|R_{O0H'} - R_{O1'H'}|$, where H′ is the hydrogen between O0 and O1′. For comparison, the gas-phase potential for proton transfer between two water molecules is also shown for each reparameterized semiempirical method.

well in the MP2 surface more closely; the OM3*n* distribution is more diffusive in the dr direction and more condensed in the R_{OO} direction. As previously discussed, OM3*n* is the most accurate semiempirical model developed in this work, and, hence, the OM3*n* distributions should be the most reliable. The results shown in Figure 13 suggest that the quality of reproducing V^{PES} will play a critical role for the successful semiempirical modeling of proton transfer in bulk water.

dx.doi.org/10.1021/ct400224n | J. Chem. Theory Comput. 2013, 9, 2672−2686

Finally, we comment on the algorithm used here to update the hydronium oxygen index (Figure 4). The acceptor O1 was the oxygen atom O1′ of the closest water molecule most of the time, but not always. Figure S14 in the Supporting Information shows plots of the distances $R_{O0O1'}$ vs R_{O0O1} at the donor−acceptor swap moments. We find $R_{O0O1'} \neq R_{O0O}$ only for a small fraction of the swaps (up to 2.7%). As such, the "special pair dancing" dynamics discussed in ref 17 can be applied here, e.g., to interpret the bimodal distribution in the solvated proton RDF $g_{O0O}(r)$ obtained from OM1*n* (see Section 3.E). The donor−acceptor distances at the swapping event display normal distributions centered at 2.37, 2.33, and 2.41 Å for the PM3*n*, OM1*n*, and OM3*n* simulations, respectively (see Figure S15 in the Supporting Information); these values match the respective locations of the well centers in V^{PES} for the corresponding semiempirical models.

4. CONCLUSION

In this paper, we have reparameterized several well-established semiempirical methods, with the objective to improve the semiempirical modeling of proton transfer in bulk water. Overall, the orthogonalization-corrected OM1*n* and OM3*n* models outperform the MNDO-based AM1*n* and PM3*n* methods in reproducing the ab initio reference geometries and energies, as well as in describing proton transfer. The OM3*n* model seems to be the most successful overall, providing radial distribution functions and potentials of mean force that are the most accurate among all methods considered. The small but finite (0.1−0.2 kcal/mol) OM3*n* free-energy barrier for proton transfer agrees with the barrier from ab initio path-integral studies.[21,27,33] The OM3*n* simulations support the Eigen−Zundel−Eigen mechanism, where a proton is transferred between resting Eigen-like structures via transitional Zundel-like structures. The success of the OM3*n* model is likely due to the resemblance between the OM3*n* potential energy surface and the effective ab initio path-integral energy surface for the Zundel ion.[21] This good match is, to some extent, fortuitous, because our reparameterization was done with regard to MP2/aug-cc-pVTZ reference data (and not with respect to the path-integral surface[21]). Future refinements of the current semiempirical surfaces are conceivable, for example, by including explicit empirical corrections for dispersion interactions.

The present work demonstrates that the semiempirical framework is robust and flexible enough to allow for realistic reparameterizations, which provide a much improved description of water and proton transfer in water. Not surprisingly, it has been easier to obtain more accurate results by starting from the improved OM*x* models with orthogonalization corrections rather than from the MNDO-based AM1 or PM3 methods. Given our choice of MP2/aug-cc-pVTZ reference data, our favored OM3*n* model is expected to provide results of MP2-like quality for water and proton transfer in water, and it should thus be useful in practice. We anticipate that it should also be possible, in principle, to reparameterize the OM*x* methods with regard to even more-accurate ab initio data (e.g., computed at the coupled-cluster level with larger basis sets).

Finally, we note that the new semiempirical models are specifically designed for water and proton transfer in water. They may or may not be more accurate than the original methods in describing other molecules or reactions. The specific reaction parametrization[45] offers a convenient way to develop computationally efficient tools with only a handful of adjustable parameters for simulations of specific systems that are too large and too expensive for density functional theory and ab initio methods to handle. Another recent example[87] is the reparameterization of AM1 for modeling the reduction of 7,8-dihydrofolate by nicotinamide adenine dinucleotide phosphate hydride in dihydrofolate reductase (DHFR). The corresponding SRP AM1 Hamiltonian was used in QM/MM simulations of the DHFR-catalyzed reaction to compute kinetic isotope effects (using a mass-perturbation-based path-integral approach), in excellent agreement with the experiment.

■ ASSOCIATED CONTENT

Ⓢ Supporting Information

Table S1 describes the optimized parameters for the currently investigated semiempirical methods. Table S2 summarizes the maxima and minima in the RDF for bulk water. Figures S1 and S2 compare the RDF computed at the MM level using the cluster model and periodic boundary conditions. The optimized geometries of the Eigen cation, the water tetramer, the Zundel ion in complex with two water molecules, and the water pentamer are shown in Figures S3−S6. Cross sections of two-dimensional potential surfaces for gas-phase proton transfer between two water molecules within a Zundel ion are illustrated in Figures S7−S11. Water dimer geometries obtained in relaxed surface scans are exemplified in Figure S12. Analyses of sample trajectories are presented in Figure S13. The distribution of R_{O1O2} vs $R_{O1O2'}$ at donor−acceptor swap events and the corresponding histogram of R_{O1O2} are displayed in Figures S14 and S15, respectively. Integrated coordination numbers are plotted in Figures S16 and S17 for water and in Figure S18 for the hydronium ion. This material is available free of charge via the Internet at http://pubs.acs.org.

■ AUTHOR INFORMATION

Corresponding Author

*E-mails: thiel@mpi-muelheim.mpg.de (W.T.), hai.lin@ucdenver.edu (H.L.).

Notes

The authors declare no competing financial interest.

■ ACKNOWLEDGMENTS

This work was supported by grants of the National Science Foundation (No. CHE0952337) and the Alexander von Humboldt Foundation to H.L.

■ REFERENCES

(1) Marx, D. *ChemPhysChem* **2006**, *7*, 1848−1870.
(2) Agmon, N. *Chem. Phys. Lett.* **1995**, *244*, 456−462.
(3) Stillinger, F. H.; David, C. W. *J. Chem. Phys.* **1978**, *69*, 1473−1484.
(4) David, C. W. *J. Chem. Phys.* **1996**, *104*, 7255−7260.
(5) Halley, J. W.; Rustad, J. R.; Rahman, A. *J. Chem. Phys.* **1993**, *98*, 4110−4119.
(6) Billeter, S. R.; van Gunsteren, W. F. *J. Phys. Chem. A* **1998**, *102*, 4669−4678.
(7) Lussetti, E.; Pastore, G.; Smargiassi, E. *Chem. Phys. Lett.* **2003**, *381*, 287−291.
(8) Mahadevan, T. S.; Garofalini, S. H. *J. Phys. Chem. B* **2007**, *111*, 8919−8927.
(9) Fogarty, J. C.; Aktulga, H. M.; Grama, A. Y.; van Duin, A. C. T.; Pandit, S. A. *J. Chem. Phys.* **2010**, *132*, 174704/1−14.
(10) Selvan, M. E.; Keffer, D. J.; Cui, S.; Paddison, S. J. *J. Phys. Chem. C* **2010**, *114*, 11965−11976.

(11) Kale, S.; Herzfeld, J.; Dai, S.; Blank, M. *J. Biol. Phys.* **2012**, *38*, 49−59.
(12) Schmitt, U. W.; Voth, G. A. *J. Phys. Chem. B* **1998**, *102*, 5547−5551.
(13) Warshel, A.; Weiss, R. M. *J. Am. Chem. Soc.* **1980**, *102*, 6218−6226.
(14) Lefohn, A. E.; Ovchinnikov, M.; Voth, G. A. *J. Phys. Chem. B* **2001**, *105*, 6628−6637.
(15) Swanson, J. M. J.; Maupin, C. M.; Chen, H.; Petersen, M. K.; Xu, J.; Wu, Y.; Voth, G. A. *J. Phys. Chem. B* **2007**, *111*, 4300−4314.
(16) Wu, Y. J.; Chen, H. N.; Wang, F.; Paesani, F.; Voth, G. A. *J. Phys. Chem. B* **2008**, *112*, 467−482.
(17) Markovitch, O.; Chen, H.; Izvekov, S.; Paesani, F.; Voth, G. A.; Agmon, N. *J. Phys. Chem. B* **2008**, *112*, 9456−9466.
(18) Vuilleumier, R.; Borgis, D. *Chem. Phys. Lett.* **1998**, *284*, 71−77.
(19) Vuilleumier, R.; Borgis, D. *J. Chem. Phys.* **1999**, *111*, 4251−4266.
(20) Sagnella, D. E.; Tuckerman, M. E. *J. Chem. Phys.* **1998**, *108*, 2073/1−2073/11.
(21) Brancato, G.; Tuckerman, M. E. *J. Chem. Phys.* **2005**, *122*, 224507/1−224507/11.
(22) Kornyshev, A. A.; Kuznetsov, A. M.; Spohr, E.; Ulstrup, J. *J. Phys. Chem. B* **2003**, *107*, 3351−3366.
(23) Park, K.; Lin, W.; Paesani, F. *J. Phys. Chem. B* **2012**, *116*, 343−352.
(24) Car, R.; Parrinello, M. *Phys. Rev. Lett.* **1985**, *55*, 2471−2474.
(25) Tuckerman, M. E.; Laasonen, K.; Sprik, M.; Parrinello, M. *J. Phys.: Condens. Matter* **1994**, *6*, A93−A100.
(26) Tuckerman, M.; Laasonen, K.; Sprik, M.; Parrinello, M. *J. Phys. Chem.* **1995**, *99*, 5749−5752.
(27) Marx, D.; Tuckerman, M. E.; Hutter, J.; Parrinello, M. *Nature* **1999**, *397*, 601−604.
(28) Asthagiri, D.; Pratt, L. R.; Kress, J. D. *Proc. Natl. Acad. Sci. U.S.A.* **2005**, *102*, 6704−6708.
(29) Chandra, A.; Tuckerman, M. E.; Marx, D. *Phys. Rev. Lett.* **2007**, *99*, 145901.
(30) Swanson, J. M. J.; Simons, J. *J. Phys. Chem. B* **2009**, *113*, 5149−5161.
(31) Tuckerman, M. E.; Chandra, A.; Marx, D. *J. Chem. Phys.* **2010**, *133*, 124108/1−22.
(32) Marsalek, O.; Elles, C. G.; Pieniazek, P. A.; Pluharova, E.; VandeVondele, J.; Bradforth, S. E.; Jungwirth, P. *J. Chem. Phys.* **2011**, *135*, 224510/1−224510/14.
(33) Marx, D.; Tuckerman, M. E.; Parrinello, M. *J. Phys.: Condens. Matter* **2000**, *12*, A153−A159.
(34) Berkelbach, T. C.; Lee, H.-S.; Tuckerman, M. E. *Phys. Rev. Lett.* **2009**, *103*, 238302/1−238302/4.
(35) Elstner, M.; Hobza, P.; Frauenheim, T.; Suhai, S.; Kaxiras, E. *J. Chem. Phys.* **2001**, *114*, 5149−5155.
(36) Choi, T. H.; Jordan, K. D. *J. Phys. Chem. B* **2010**, *114*, 6932−6936.
(37) Maupin, C. M.; Aradi, B. l.; Voth, G. A. *J. Phys. Chem. B* **2010**, *114*, 6922−6931.
(38) Riccardi, D.; Konig, P.; Prat-Resina, X.; Yu, H. B.; Elstner, M.; Frauenheim, T.; Cui, Q. *J. Am. Chem. Soc.* **2006**, *128*, 16302−16311.
(39) Goyal, P.; Elstner, M.; Cui, Q. *J. Phys. Chem. B* **2011**, *115*, 6790−6805.
(40) McNamara, J. P.; Hillier, I. H. *Phys. Chem. Chem. Phys.* **2007**, *9*, 2362−2370.
(41) Řezáč, J.; Fanfrlík, J. i.; Salahub, D.; Hobza, P. *J. Chem. Theory Comput.* **2009**, *5*, 1749−1760.
(42) Korth, M. *J. Chem. Theory Comput.* **2010**, *6*, 3808−3816.
(43) Korth, M. *ChemPhysChem* **2011**, *12*, 3131−3142.
(44) Gaus, M.; Cui, Q.; Elstner, M. *J. Chem. Theory Comput.* **2011**, *7*, 931−948.
(45) Gonzalez-Lafont, A.; Truong, T. N.; Truhlar, D. G. *J. Phys. Chem.* **1991**, *95*, 4618−4627.
(46) Dewar, M. J. S.; Zoebisch, E. G.; Healy, E. F.; Stewart, J. J. P. *J. Am. Chem. Soc.* **1985**, *107*, 3902−3909.
(47) Stewart, J. J. P. *J. Comput. Chem.* **1989**, *10*, 209−220.
(48) Stewart, J. J. P. *J. Comput. Chem.* **1989**, *10*, 221−264.
(49) Dewar, M. J. S.; Thiel, W. *J. Am. Chem. Soc.* **1977**, *99*, 4899−4907.
(50) Kolb, M.; Thiel, W. *J. Comput. Chem.* **1993**, *14*, 775−789.
(51) Weber, W.; Thiel, W. *Theor. Chem. Acc.* **2000**, *103*, 495−506.
(52) Scholten, M. Doctoral Thesis, University of Düsseldorf, Düsseldorf, Germany, 2003.
(53) Otte, N.; Scholten, M.; Thiel, W. *J. Phys. Chem. A* **2007**, *111*, 5751−5755.
(54) Korth, M.; Thiel, W. *J. Chem. Theory Comput.* **2011**, *7*, 2929−2936.
(55) Møller, C. M. S.; Plesset, M. S. *Phys. Rev.* **1934**, *46*, 618−622.
(56) Dunning, J. T. H. *J. Chem. Phys.* **1989**, *90*, 1007−1023.
(57) Woon, D. E.; Thom H. Dunning, J. *J. Chem. Phys.* **1994**, *100*, 2975−2988.
(58) Ramírez, F.; Hadad, C. Z.; Guerra, D.; David, J.; Restrepo, A. *Chem. Phys. Lett.* **2011**, *507*, 229−233.
(59) Pérez, J. F.; Hadad, C. Z.; Restrepo, A. *Int. J. Quantum Chem.* **2008**, *108*, 1653−1659.
(60) Stull, D. R.; Prophet, H. In *National Standard Reference Data Series (United States, National Bureau of Standards)*; National Bureau of Standards (NBS): Washington, DC, 1971; Vol. *37*.
(61) Lias, S. G.; Liebman, J. F.; Levin, R. D. *J. Phys. Chem. Ref. Data* **1984**, *13*, 695−808.
(62) Frisch, M. J.; Trucks, G. W.; Schlegel, H. B.; Scuseria, G. E.; Robb, M. A.; Cheeseman, J. R.; Scalmani, G.; Barone, V.; Mennucci, B.; Petersson, G. A.; Nakatsuji, H.; Caricato, M.; Li, X.; Hratchian, H. P.; Izmaylov, A. F.; Bloino, J.; Zheng, G.; Sonnenberg, J. L.; Hada, M.; Ehara, M.; Toyota, K.; Fukuda, R.; Hasegawa, J.; Ishida, M.; Nakajima, T.; Honda, Y.; Kitao, O.; Nakai, H.; Vreven, T.; Montgomery Jr., J. A.; Peralta, J. E.; Ogliaro, F.; Bearpark, M.; Heyd, J. J.; Brothers, E.; Kudin, K. N.; Staroverov, V. N.; Keith, T.; Kobayashi, R.; Normand, J.; Raghavachari, K.; Rendell, A.; Burant, J. C.; Iyengar, S. S.; Tomasi, J.; Cossi, M.; Rega, N.; Millam, J. M.; Klene, M.; Knox, J. E.; Cross, J. B.; Bakken, V.; Adamo, C.; Jaramillo, J.; Gomperts, R.; Stratmann, R. E.; Yazyev, O.; Austin, A. J.; Cammi, R.; Pomelli, C.; Ochterski, J. W.; Martin, R. L.; Morokuma, K.; Zakrzewski, V. G.; Voth, G. A.; Salvador, P.; Dannenberg, J. J.; Dapprich, S.; Daniels, A. D.; Farkas, O.; Foresman, J. B.; Ortiz, J. V.; Cioslowski, J.; Fox, D. J.; Version B.01. Gaussian, Inc.: Wallingford, CT, 2010.
(63) Thiel, W.; Version 7.0. Max-Planck-Institut für Kohlenforschung: Mülheim an der Ruhr, Germany, 2005.
(64) Stewart, J. P. *J. Mol. Model.* **2007**, *13*, 1173−1213.
(65) Hofer, T. S.; Hitzenberger, M.; Randolf, B. R. *J. Chem. Theory Comput.* **2012**, *8*, 3586−3595.
(66) Warshel, A.; Levitt, M. *J. Mol. Biol.* **1976**, *103*, 227−249.
(67) Field, M. J.; Bash, P. A.; Karplus, M. *J. Comput. Chem.* **1990**, *11*, 700−733.
(68) Gao, J., Thompson, M. A., Eds. *Combined Quantum Mechanical and Molecular Mechanical Methods*; ACS Symposium Series 712; American Chemical Society: Washington, DC, 1998.
(69) Zhang, Y.; Lee, T.-S.; Yang, W. *J. Chem. Phys.* **1999**, *110*, 46−54.
(70) Gogonea, V.; Westerhoff, L. M.; Merz, K. M., Jr. *J. Chem. Phys.* **2000**, *113*, 5604−5613.
(71) Sherwood, P. In *Modern Methods and Algorithms of Quantum Chemistry*; Grotendorst, J., Ed.; John von Neumann-Instituts: Jülich, Germany, 2000; Vol. *3*, pp 285−305.
(72) Lin, H.; Truhlar, D. G. *Theor. Chem. Acc.* **2007**, *117*, 185−199.
(73) Senn, H. M.; Thiel, W. *Top. Curr. Chem.* **2007**, *268*, 173−290.
(74) Berendsen, H. J. C.; Postma, J. P. M.; von Gunsteren, W. F.; Hermans, J. In *Intermolecular Forces*; Pullman, B., Ed.; D. Reidel Publishing Company: Dordrecht, The Netherlands, 1981; pp 331−342.
(75) Bakowies, D.; Thiel, W. *J. Phys. Chem.* **1996**, *100*, 10580−10594.
(76) Lin, H.; Zhang, Y.; Pezeshki, S.; Truhlar, D. G. QMMM, Version 1.4.0.CO; University of Minnesota: Minneapolis, MN, 2012.
(77) Ponder, J. W. TINKER, Version 5.1; Washington University: St. Louis, MO, 2010.

(78) Nosé, S. *Mol. Phys.* **1982**, *52*, 255−268.
(79) Hoover, W. G. *Phys. Rev. A* **1985**, *31*, 1695−1697.
(80) Jorgensen, W. L.; Chandrasekhar, J.; Madura, J. D.; Impey, R. W.; Klein, M. L. *J. Chem. Phys.* **1983**, *79*, 926−935.
(81) Thiel, W. In *Theory and Applications of Computational Chemistry*; Dykstra, C. E., Frenking, G., Kim, K. S., Scuseria, G. E., Eds.; Elsevier: Amsterdam, 2005; pp 559−580.
(82) Tuttle, T.; Thiel, W. *Phys. Chem. Chem. Phys.* **2008**, *10*, 2159−2166.
(83) Grimme, S. *J. Comput. Chem.* **2006**, *27*, 1787−1799.
(84) Soper, A. K. *Chem. Phys.* **2000**, *258*, 121−137.
(85) Soper, A. K.; Benmore, C. J. *Phys. Rev. Lett.* **2008**, *101*, 065502/1−065502/4.
(86) Head-Gordon, T.; Johnson, M. E. *Proc. Natl. Acad. Sci. U.S.A.* **2006**, *103*, 7973−7977.
(87) Doron, D.; Major, D. T.; Kohen, A.; Thiel, W.; Wu, X. *J. Chem. Theory Comput.* **2011**, *7*, 3420−3437.